Article

Tissue Engineering Scaffold Material with Enhanced Cell Adhesion and Angiogenesis from Soy Protein Isolate Loaded with Bio Modulated Micro-TiO$_2$ Prepared via Prolonged Sonication for Wound Healing Applications

Rekha Rose Koshy, Siji K. Mary, Arunima Reghunadhan, Yogesh Bharat Dalvi, Lekshmi Kailas, Nereida Cordeiro, Sabu Thomas, and Laly A. Pothen*
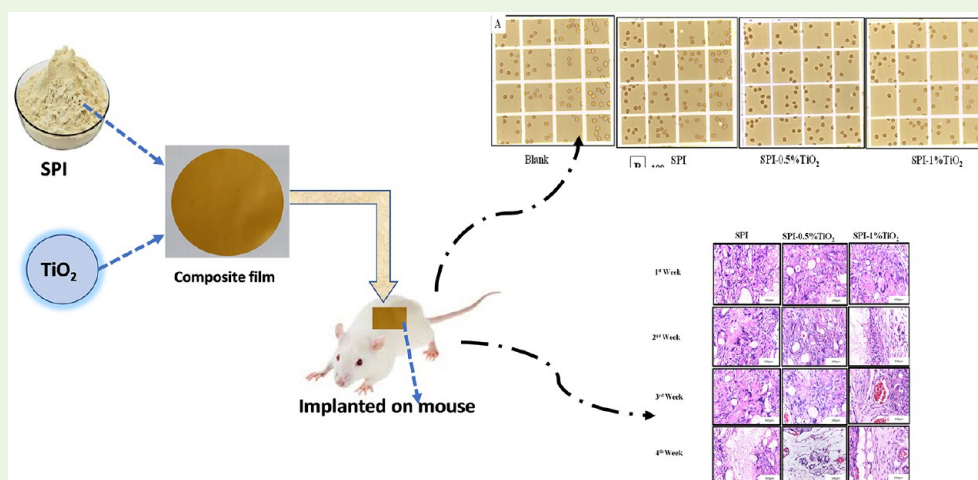
Cite This: ACS Biomater. Sci. Eng. 2022, 8, 4896−4908

Read Online

ACCESS | Metrics & More | Article Recommendations | SI Supporting Information

ABSTRACT: Tissue engineering is a technique that promotes healing by creating an ideal environment for endogenous cells to migrate and grow into the site of injury via a scaffold, improving regeneration and reducing the time required for in vitro cell culture. In this work, the effect of the addition of sonicated TiO$_2$ in the soy protein isolate (SPI) matrix for tissue engineering applications was studied. In comparison to adding expensive nano TiO$_2$, this method of incorporating sonicated TiO$_2$ into the SPI matrix will aid in achieving improved properties at a lower cost. The effect of the addition of sonicated TiO$_2$ on the morphological, UV transmittance, mechanical, thermal, surface energy, and hydrophilicity of SPI films was investigated. The result shows that the uniformly distributed TiO$_2$ particles successfully blocked 95% of UV light. Scanning electron microscopy revealed a significant reduction in the TiO$_2$ agglomerate size and homogeneous distribution of the same when sonication was applied instead of mechanical dispersion. A simultaneous increase of tensile strength (from 3.16 to 4.58 MPa) and elongation at break values (from 24.25% to 95.31%) with 0.5% TiO$_2$ was observed. The addition of 0.25% TiO$_2$ was found to significantly enhance the elongation at break value to 120.83%. Incorporation of micro-TiO$_2$ particles could improve the surface roughness, surface energy, and wettability of SPI films. In vitro cell adhesion studies and in vivo subcutaneous implantation studies were performed to assess the cell growth and angiogenesis of the developed film membranes. An MTT assay showed that SPI-1%TiO$_2$ film favored cell viability up to 118%, and in vivo subcutaneous implantation studies showed enhanced cell growth and angiogenesis for SPI-1% TiO$_2$ films. This SPI-TiO$_2$ film with enhanced surface properties can be used as an ideal candidate for tissue engineering applications.

**KEYWORDS:** SPI, TiO$_2$, cell adhesion, sonication, tissue engineering
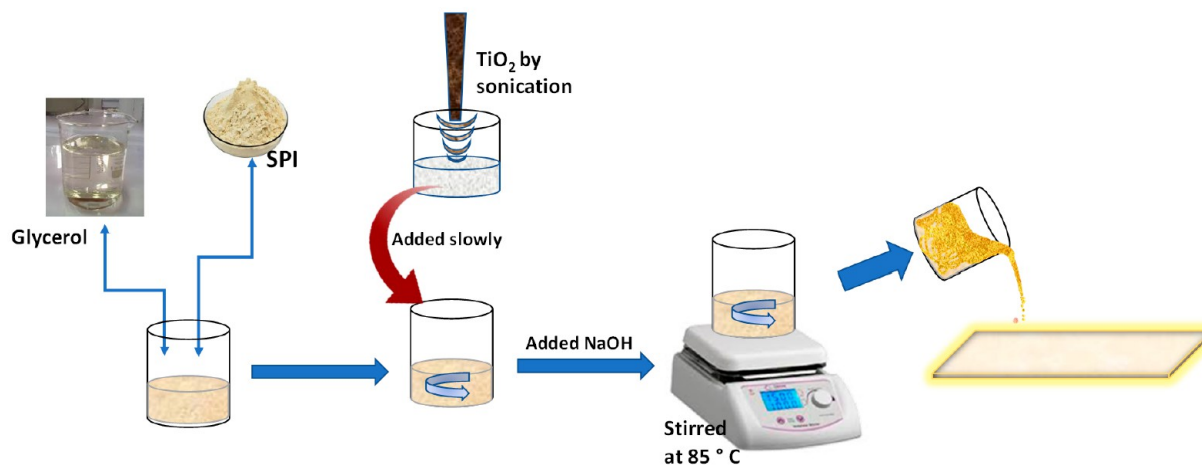
1. INTRODUCTION

The technique, tissue engineering, is a combination of regeneration and repair of cells and tissues by incorporating various materials that are compatible with the body. A considerable amount of progress has been made in this field, both in the development of new tools and in converting
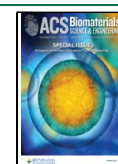
Scheme 1. Preparation Scheme of SPI-TiO$_2$ Films

various biomaterials to functional tissue engineered products.[1] However, conventional tissue-engineering techniques, which use prefabricated scaffolds for implantation at the injury site, require a lot of time and labor. In this context, in situ tissue engineering was proposed to overcome the limitations of cell-based tissue engineering by utilizing the body's own regenerative capabilities. A good target-specific scaffold should interact with the living cells, resulting in long-lasting survival and promoting vascularization.[2] The use of bioactive materials in scaffolds is found to favorably increase vascularization without the need to add an external growth factor. Titanium dioxide (TiO$_2$) is one such bioactive material that is reported to have the potential to induce angiogenesis.[3] The ability of TiO$_2$ to promote angiogenesis is attributed to the development of reactive oxygen species radicals on exposure to light. TiO$_2$ is commonly used as a photocatalyst owing to its strong oxidizing abilities, chemical stability, super hydrophilicity, nontoxicity, sturdiness, low cost, and transparency under visible light.[4] The majority of the reported work used nanoscale titania as a filler and is very expensive. In comparison with TiO$_2$ nano powder, TiO$_2$ microscale structures have higher surface areas, more tunable opening(pore) structures, and better photocatalytic activity.[5] The microscale titania can be produced by the simple ultrasonication process in a probe sonicator from its macro precursor. In this sonication process, the filler is subjected to a high shear process using ultrasonic energy. Passing ultrasonic waves through the filler solution results in the formation of high pressure, which breaks the filler into a small size. Dispersion using ultrasonic waves is also being used to break the binding energy of particles without the need for any external chemical agents.

Several studies have been published on the use of TiO$_2$ nanoparticle reinforced biopolymeric matrices as biomaterials. There have been few or no reports on the use of micro-TiO$_2$ particles as frameworks for tissue engineering applications. As a result, in this study, we reinforced a protein-based polymeric material with micro-TiO$_2$ and assessed its potential for use as a biomaterial. Protein-based biopolymeric matrices have been reported to exhibit superior biological behavior when compared to polysaccharides due to the presence of polypeptide chains containing reactive amino acids.[6] Soy protein isolate (SPI) is one such plant-based protein, which when reinforced with suitable bioactive fillers, finds excellent

applicability in the biomedical field.[7] SPI, being a naturally occurring protein can recapitulate the physiochemical and biological features of the native extracellular matrix (ECM), thereby achieving the highest level of biomimicry.[8] Because of their inherent functional groups and nutrient ingredients, SPI-based biomaterials have been shown in studies to stimulate cell growth without the need for additional growth factors.[6] Furthermore, SPI-based materials can promote collagen formation by fibroblasts and thus have significant wound healing potential. As a result, the effect of sonicated TiO$_2$ on the potential of SPI as a biomaterial is being investigated.

Before entering into in vivo applications with SPI-based composites, the surface biological characteristics must be thoroughly investigated. SPI-like biomaterials should exhibit not only biocompatibility and biostability but also specific surface biological characteristics that can induce positive cell responses. Surface roughness and morphology have a significant impact on the biomaterial's surface energy, which improves tissue growth and cell responses. Surface roughness is well-thought-out to influence the reactions of adherent cells, especially in the case of body implants, and an efficient design is a rough topographic surface. Previous studies have shown that TiO$_2$ composites with high surface roughness can promote epithelial growth and attachment of fibroblasts.[9,10]

This study examined the impact of sonicated TiO$_2$ on the optical, mechanical, and thermal properties of SPI films. The ability of the produced SPI-TiO$_2$ film for tissue engineering applications was investigated in particular. The effect of the addition of sonicated TiO$_2$ on the surface properties like roughness, surface energy, hydrophilicity, adsorption, and diffusion coefficient of the SPI film was studied. Also, distinct from TiO$_2$ nanopowder, TiO$_2$ microscale structures have a higher surface area, more tunable pore structures, and improved photocatalytic activity. The ability of the scaffolds to enhance cell adhesion, migration, and proliferation of endogenous cells that facilitate repair was monitored. The ability of the scaffolds to stimulate the production of cell proliferative and angiogenic factors that can enhance cell growth and vascularization was assessed using in vivo and in vitro models.

2. MATERIALS AND METHODS

2.1. Materials. TiO_2 macroparticles (rutile) were purchased from Merck. The protein isolate (SPI, 98 wt % protein) was obtained from Adeesh Agrofoods (Haryana, India). All reagents used were of analytical rating. Deionized water was used for all sample preparations.

2.2. Preparation of SPI/TiO_2 Films. The isolate powder was liquified using 200 mL of distilled water that contained 3.6 mL of glycerol as the plasticizing agent to create the SPI solution. TiO_2 dispersions in the desired quantity were combined with the SPI solution and agitated for 10 min. 0.25%, 0.5%, 0.75%, and 1% of TiO_2 solutions previously sonicated for 1 h were added in varying amounts. TiO_2 was added very gradually while being vigorously stirred into the protein solution in order to achieve a proper dispersion.

The pH of the resulting solutions was attuned to 10 ± 0.1 with 1 N sodium hydroxide. The solutions were then kept at 85 °C for 20 min, emptied onto a Teflon pan, and dehydrated at 55 °C for 12 h in a vacuum oven (Scheme 1). After drying, the films were peeled off and stored at $43 \pm 2\%$ RH and 25 ± 2 °C for 24 h prior to testing.

2.3. Appearance and Color Parameters of SPI-TiO_2 Films. The color parameters of the film sample were measured with an SC-80C colorimeter, and its L (lightness), a (redness to greenness), and b (yellowness to blueness) values were determined. L can have values from 0 (black) to 100 (pure white). a can have a value from negative (green) to positive (red), and b can assume value from negative (blue) to positive (yellow; Luchese et al.)

2.4. Scanning Electron Microscope (SEM). The surface morphology of sonicated and nonsonicated TiO_2 solutions and SPI-TiO_2 films was done using a TESCAN Vega-3 scanning electron microscope (5.0 kV accelerating voltage).

2.5. Thickness Measurements. For the thickness measurement of the specimens, a screw gauge with a correctness of 0.01 mm was used. The measurement was carried out at five randomly selected points of the sample film and was measured for each specimen. The result were plotted by considering the mean values.

2.6. Intrinsic Fluorescence Spectroscopy. The fluorescence of SPI-TiO_2 films was analyzed at room temperature (25 ± 1 °C) using a Carry 50 Fluoro spectrophotometer (Varian, USA). Excitation and emission slits used for the experiments were 10.0 and 20.0 nm, respectively, with an excitation wavelength of 290 nm and emission spectra from 305 to 450 nm. Each sample had three scans.

2.7. Ultra Violet Spectroscopy (UV). The absorbance spectrum (200−700 nm) of the films was documented using a UV mini-1240 spectrophotometer (Shimadzu, Kyoto, Japan). The sample was cut into a rectangular-shaped piece and placed in the spectrophotometer test cell, and air was used as the reference.

2.8. FTIR Analysis. FTIR spectroscopy was conducted on a PerkinElmer Spectrum 100 spectrometer with a Universal ATR accessory. IR spectra were collected from the samples within the range of $4000-650$ cm^{-1}, Two areas were analyzed per sample, and 50 scans were recorded per spectra. A background spectrum was recorded under the same experimental conditions and subtracted from each spectrum presented. An automatic baseline correction was done as postprocessing for all spectra.

2.9. XRD Analysis. The crystal structures of the micro-TiO_2 particles and the composite films were obtained using a D8 Advance Polycrystal X-ray diffractometer (Bruker, Germany) with a nickel-filtered Cu Kα radiation beam in the angular range of 6−70 (2θ) at a voltage of 40 kV and a current of 40 mA.

2.10. Atomic Force Microscopy (AFM). AFM observations were carried out in the air on as-received sample surfaces using an Agilent 5500 AFM operated in contact mode. Measurements were carried out using standard triangular silicon nitride cantilevers (MSCT from Bruker). Topography, deflection, and friction data were collected simultaneously. The images were taken at 512×512 pixels resolution. Two areas of 50×50 μm were imaged per sample.

2.11. Inverse Gas Chromatography (IGC). IGC measurements were taken on an automatized inverse gas chromatograph (Surface Measure Systems London, UK), equipped with both thermal

conductivity (TCD) and flame ionization (FID) detectors. The specifications were according to Cordeiro et al.[11]

2.12. Moisture Sorption Studies. Films were divided into tiny pieces and predried for 1 week at room temperature on silica in a vacuum. With saturated salt solutions of $MgCl_2$, $MgNO_3 \cdot 6H_2O$, and $Na_2SO_4 \cdot 10H_2O$, environments with constant relative humidities of 32, 53, and 95%, respectively, were created within the desiccators. These RH gradient values were selected because they correspond to most of the gradient observed within food materials or between packaged foods and surrounding media. The weights of the sample were checked until equilibrium was attained. The moisture absorption of the samples was calculated as follows:

$$\text{Moisture absorption} = \frac{(w1 - wo)}{wo} \times 100 \quad (1)$$

where wo and w1 were the weights of the sample before exposure to different relative humidities and after equilibrium, respectively. The average of three replicates of each sample was taken.[12] The results are given in the Supporting Information.

2.13. Contact Angle. Contact angle measurement was done in a water contact angle instrument, SEO Phoenix 300, using software-8. Then, 6−7 μL drops of deionized water were placed on the surface of each film using a computer controlled microsyringe system under ambient conditions (temperature of 20 °C, relative humidity of 50%). The tangent angle formed between the film surface and the liquid drop was measured as the contact angle, and the drop image was captured using a CCD camera. Five different positions were tested for each film and the average taken.

2.14. Hemocompatibility Studies. To evaluate the blood compatibility of the film samples, a hemolysis assay and red blood cell aggregation studies were done. Appropriate protocols were followed for taking blood samples from willing patients. An experiment was carried out according to the procedure followed by Augustine et al.[13]

2.15. In Vitro Cytotoxicity Assay. The MTT assay was used for the assessment of cell proliferation (L929 fibroblasts) as reported in the earlier studies.[13] Various SPI scaffold stocks (25 mg/10 mL) were prepared in DMEM. After incubation for 24 h, the suspension was centrifuged at 2000 rpm for 10 min, and the supernatant was filtered using a syringe filter and incubated with cells (ISO 10993-5, 2009) and further incubated for different timelines (24, 48, and 72 h).

2.16. In Vivo Experimental Design. In this study, there is a total of four experimental solvent cast SPI membranes: (1) SPI alone, (2) SPI blended with TiO_2 (1%), (3) SPI blended with CTE (7%), and (4) SPI blended with TiO_2 (1%) and CTE (7%).

Before implantation, the SPI membranes were cut into 1×1 cm and sterilized using ethylene oxide (EtO). Animal experiments were designed and carried out as recommended in ISO 10993, part 6 (2016) with the approval of the Institutional Animal Ethics Committee of the host institution. Adult male Sprague−Dawley rats having a weight between 250 and 350 g were used for the study. The rats were provided with standard environmental controlled conditions of 25 ± 3 °C, a 12 h light-dark cycle, standard laboratory animal feed, and UV-sterile water. A total of 16 rats were randomized into four groups ($n = 4$) for subcutaneous implantation of SPI membranes, with (TiO_2/CTE) and without (blank).

On the day of surgery, rats were anesthetized by an intramuscular injection of 5% xylazine (10 mg/kg of the body weight) and 10% ketamine hydrochloride (80 mg/kg of the bodyweight). The hairs on the dorsum of the rats were shaved with a Philips electric pet care trimmer, and the skin was cleaned using a 2% povidone−iodine solution. A linear incision of 8 mm length was made on the dorsum of the rat using a carbon steel surgical blade no. 15, and the full-thickness flap was elevated. All four sterile scaffolds were implanted and fixed using absorbable 3−0 catgut suture and were closed by giving interrupted sutures with number 3−0 black braided silk. In postoperative care, for 3 days, ceftriaxone (20 mg/kg) and meloxicam (0.5 mg/kg) were administered IM as an antibiotic and analgesic, respectively. The implanted scaffold samples were harvested by euthanizing four rats from each group in a CO_2 chamber at the first,

second, third, and fourth weeks. The connective tissue surrounding scaffolds was fixed in 10% formalin for histological evaluation. All sections were stained with Harris's hematoxylin and eosin (H&E) stain for histological analysis. After H&E staining, sections were investigated histologically by observation under a polarized optical microscope (Leica DM 4500 P LED), and the images were captured. Sections were viewed and scored by a blinded pathologist using a four-point scoring system (0 absent, + mild, ++ moderate, and +++ severe) to determine the tissue reaction and membrane degradation.

2.17. Statistical Analysis. One-way analysis of variance (ANOVA) was performed with Duncan's multiple range tests using the SPSS statistical analysis reference.

3. RESULTS AND DISCUSSION

3.1. Appearance and Color Parameters of SPI-TiO$_2$ Films. The photographs of (a) pure SPI film and (b) that
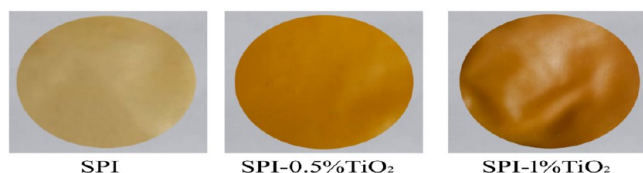
**Figure 1.** Film appearance of SPI and SPI composite films.

Table 1. Color Parameters of SPI-TiO$_2$ Films[a]

samples	L	a	b
SPI	73.33 ± 1.53[a]	3.93 ± 1.05[b]	20.67 ± 2.08[c]
0.5%TiO$_2$	59.06 ± 1.10[b]	11.10 ± 1.15[a]	38.33 ± 1.53[a]
1%TiO$_2$	60.67 ± 3.21[b]	10.33 ± 3.51[a]	33.00 ± 2.64[b]

[a]Standard deviation (±) is given. Different small case letters within the same column indicate significant differences ($p < 0.05$).

containing 1% TiO$_2$ are shown in Figure 1. All of the films were smooth and homogeneous. The pure SPI film was see-through while the film containing 1% TiO$_2$ was translucent. It is observed that the transmittance decreases with an increasing concentration of TiO$_2$ in the protein matrix. This can be attributed to the great specific surface area and increased

Scheme 2. Illustration Showing the Breakdown of Macroscale Titania to Microscale by Sonication and the Resultant Particles Uniformly Distributed in the SPI Matrix
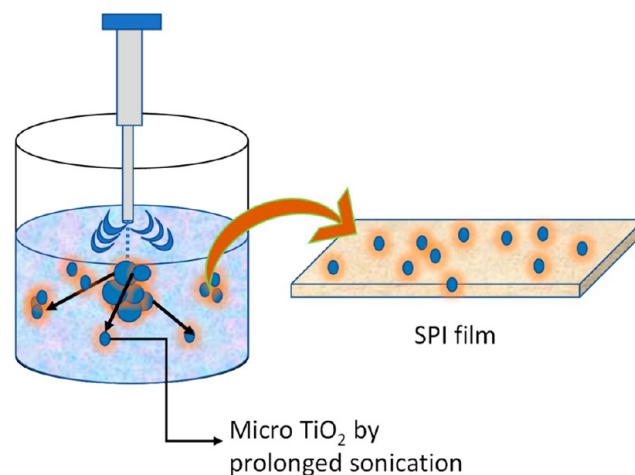
refractive index of the sonicated TiO$_2$ particles resulting in diffuse reflection of light from the film surface.[14]Table 1 shows the color parameter values. L values show that lightness decreased with the increased addition of TiO$_2$ in the matrix. An increase in the value showed the color change to red/brown. The film's hue changed from blue to yellow as the b value grew.

3.2. SEM Analysis of TiO$_2$ and SPI-TiO$_2$ Films. Sonochemical synthesis of microparticles from macroparticles involves the application of ultrasound radiation (20 kHz-10 MHz) to form acoustic cavitation, i.e., the formation, growth, and impulsive collapse of bubbles that will generate hotspots, with high temperature (5000−25 000 K) and pressure (of more than 1000 atm). This high local pressure and temperature, combined with rapid cooling, provides a one-of-a-kind method of synthesis of microparticles.

From the SEM analysis of the TiO$_2$ solution (Figure 2a and b), it is clear that after sonication for 1 h, the spherical particles of TiO$_2$ have been homogenized and the particle density has
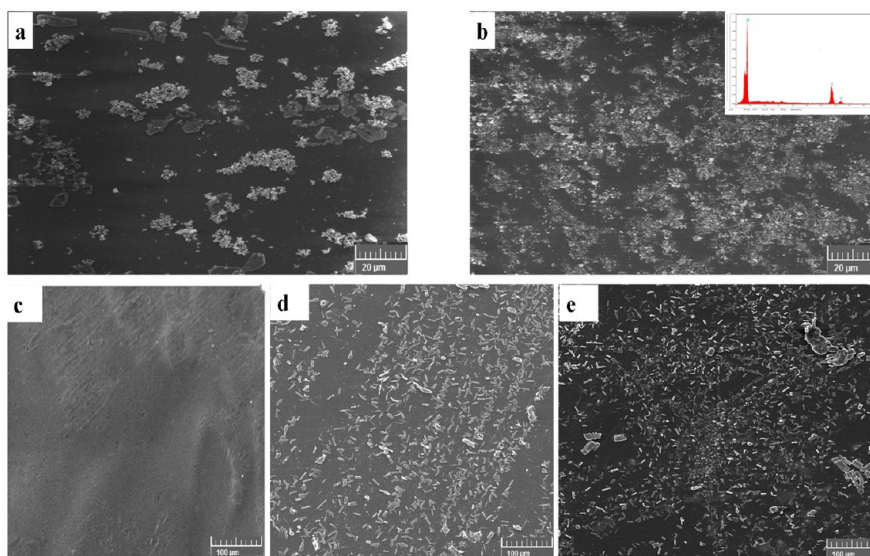
Figure 2. SEM images of TiO$_2$ (a) before and (b) after sonication for 1 h. (Inset image in b shows the EDX spectra of TiO$_2$.) SEM images of composite films (c) SPI, (d) SPI-0.5% TiO$_2$, (e) SPI-1% TiO$_2$.
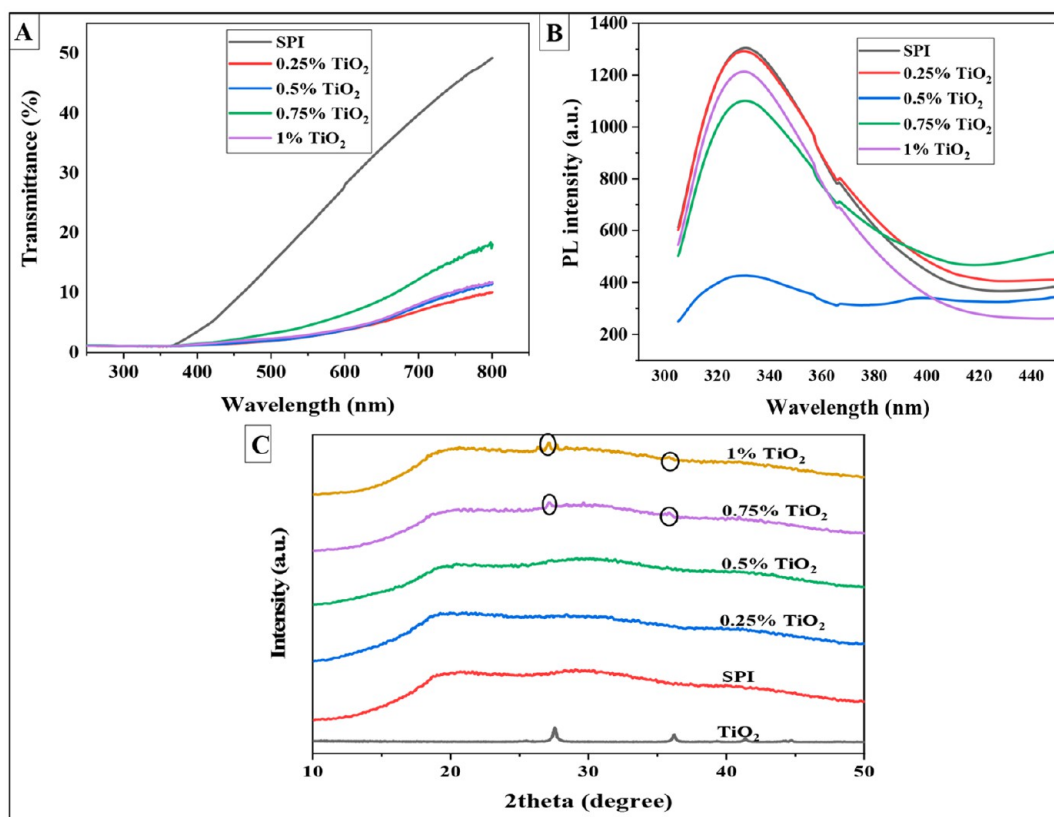
Figure 3. (A) UV–visible spectrum. (B) Photoluminescence emission and (C) X-ray diffraction of SPI-TiO₂ composite films.
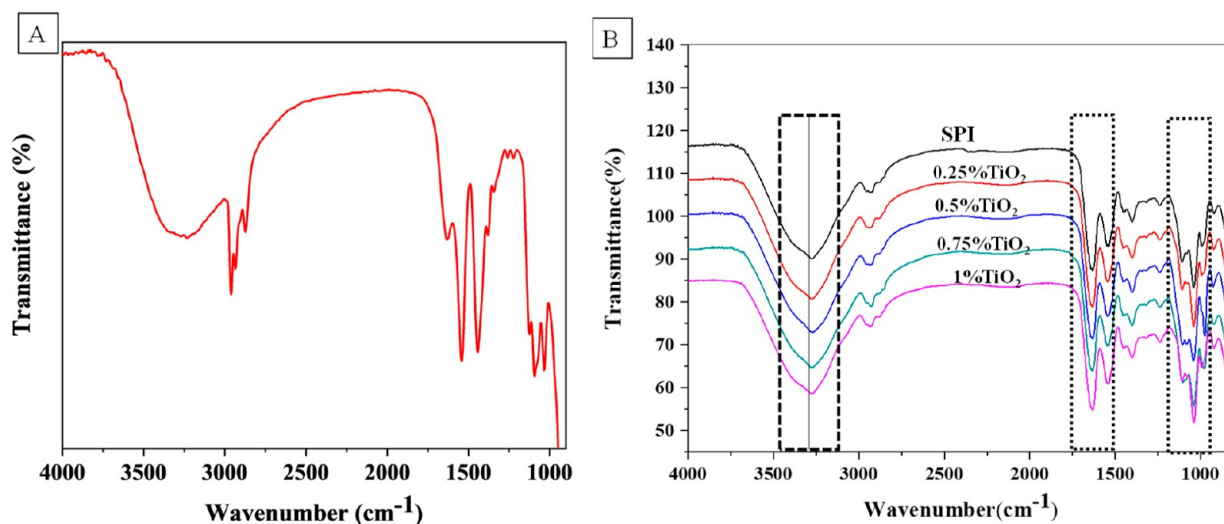

Figure 4. (A) FTIR of (A) TiO_2 powder and (B) SPI-TiO_2 composite films.

decreased when compared to a solution which has not been syndicated. The microstructure of nonsonicated TiO_2 samples showed the appearance of particle agglomerates and or large clusters, while after sonication a homogeneous dispersion of particles was achieved (Scheme 2). Here in Figure 2b, the size of the aggregates is reduced and individual particles or smaller clusters are formed. The average particle size was 180 to 205 nm. The inset image in b shows the EDX spectra of TiO_2, which contains only the peaks of Ti and O.

Figure 2c,d,e show the SEM images of the surface of the pure SPI and the TiO_2/SPI composite films. On examining the

virgin SPI film surface, it seems to be even and devoid of any contamination. The physical appearance of the SPI film is thus supported by the morphology on the microscale. Thus, it can be simply said that the surface morphology of the pure SPI film was smooth and homogeneous. When moving to the composite films, a granular structure on the surface of the films appeared where TiO_2 was incorporated (Figure 2d,e). On close examination, the SEM images reveal rod-shaped TiO_2 microparticles that are homogeneously distributed in the matrix at 0.5% concentration and that tend to form small agglomerates as the concentration increases to 1%. Even then
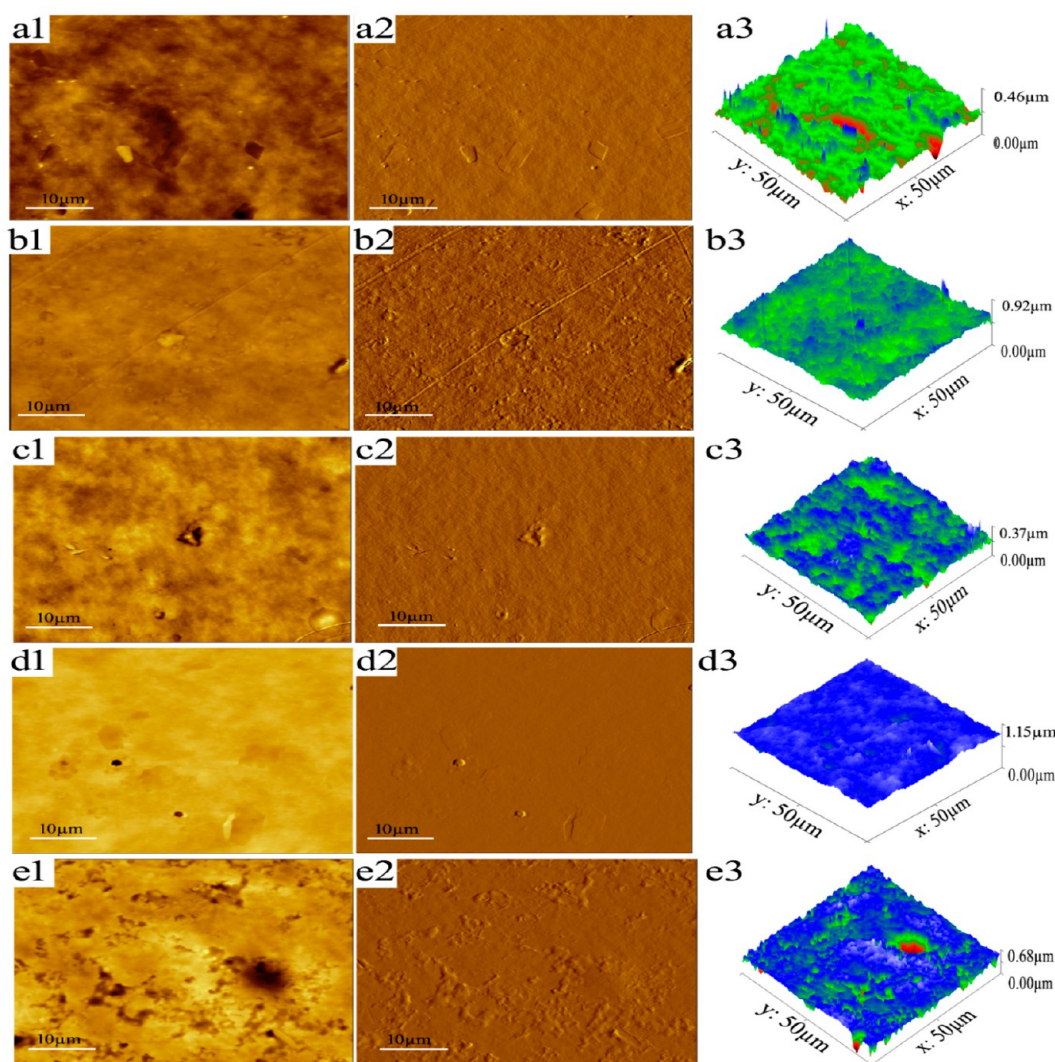
Figure 5. AFM topography and deflection images and the 3D view of the sample surface of control SPI (a), SPI-0.25%TiO$_2$ (b), SPI-0.5%TiO$_2$ (c), SPI-0.75%TiO$_2$ (d), and SPI-1%TiO$_2$ (e). The scale bar in the topography images corresponds to 10 μm.

Table 2. Surface Roughness, Surface Energy (Dispersive, Specific, and Total), Adsorption Potential Maxima (A_{max}) and Diffusion Coefficient (D_p) of the SPI-TiO$_2$ Samples[a]

sample	surface roughness	Υ_S^{sp}	Υ_S^d(mJ/m^2)	Υ_S^{total}	A_{max}(kJ/mol)	D_p	K_a	K_b	K_a/K_b
SPI	38.05[b]	19.11[a]	38.43[a]	57.53[a]	9.90[a]	0.07[a]	0.06[a]	0.20[a]	0.30[a]
0.25%TiO$_2$	33.05[bc]	25.89[b]	39.45[a]	65.34[abc]	9.86[a]	0.41[bc]	0.08[b]	0.16[b]	0.49[b,c]
0.5% TiO$_2$	24.20[c]	25.35[b]	39.25[a]	64.59[abc]	10.00[a]	0.45[c]	0.08[b]	0.16[b,c]	0.48[b,c]
0.75%TiO$_2$	29.70[bc]	30.99[c]	36.18[a]	67.17[c]	8.88[ab]	0.39[b]	0.08[b,c]	0.15[b,c]	0.55[c,d]
1%TiO$_2$	63.05[a]	31.44[c]	35.30[a]	66.74[bc]	7.89[b]	0.28[d]	0.09[c]	0.16[b,c]	0.60[e]

[a]Different small case letters within the same column indicate significant differences ($p < 0.05$).

the dispersion of the particles is nearly uniform, and they appear as particles in the matrix.

3.3. UV−Visible Transmittance Spectra. To evaluate the interaction between SPI-TiO$_2$ films and UV light radiation, UV−visible transmittance spectra of the composite films were taken. Figure 3A shows the UV transmittance spectra of the SPI/TiO$_2$ composite films with different TiO$_2$ concentrations. Due to the absorption of UV radiation by the aromatic amino acid groups of the proteins, the control SPI film has good UV blocking properties in the range 200−320 nm (UV-B and UV-C)[15] but poor UV-blocking activity in the UV-A range (320−400 nm).[16] The incorporation of TiO$_2$ into the SPI films

caused a significant ($p < 0.05$) decline in the transmittance (T) in the UV-A, UV-B, and UV-C regions.[17] More than 95% of UV light was prevented by even a 0.25% TiO$_2$ addition into the film. Thus, the incorporation of TiO$_2$ prevents free radical formation under UV light. It has also been reported by Li et al.[18] that the addition of TiO$_2$ into whey protein isolate led to the decline of transmission in the visible, UVA, and UVB regions, and these declines showed a first-order exponential decay depending on TiO$_2$ concentration.

3.4. Fluorescence Spectroscopy. The fluorescence spectra of the composite films with different TiO$_2$ contents are shown in Figure 3B. The maximum emission wavelength of
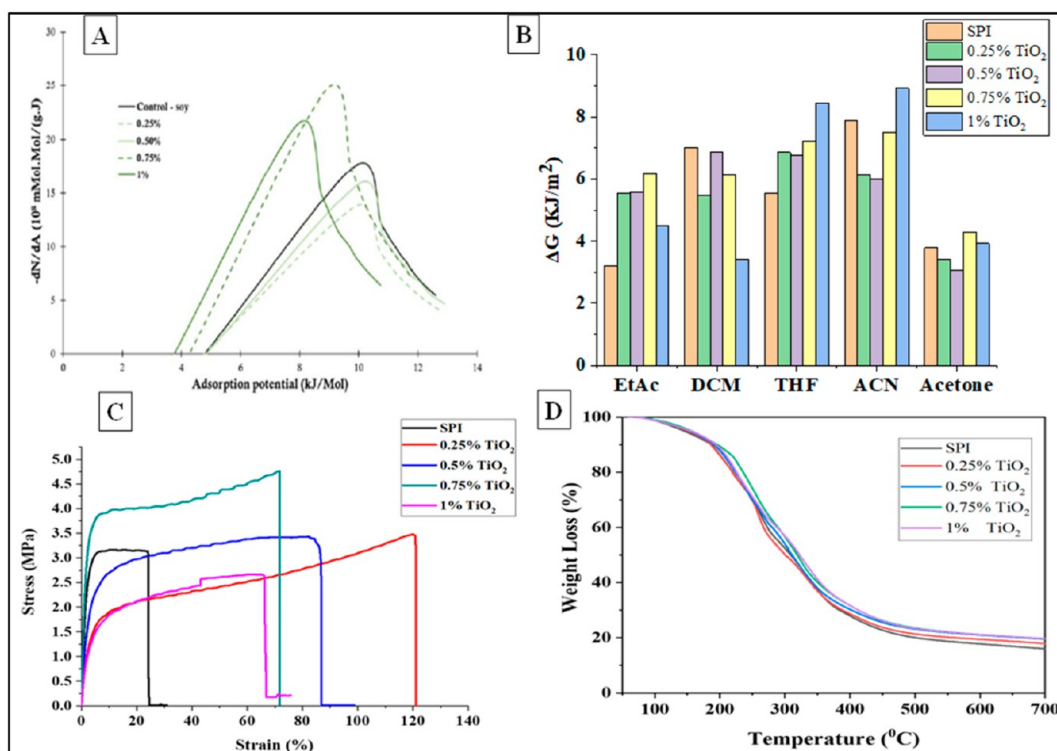
Figure 6. (A) Heterogeneity profile of *n*-octane into the SPI-TiO$_2$ samples at 298 K. (B) Polar interactions between the polar probes with the SPI-TiO$_2$ samples at 298 K. EtAc, ethyl acetate; DCM, dichloromethane; THF, tetrahydrofuran; ACN, acetonitrile. (C) Stress−strain graph, (D) TG curves of SPI-TiO$_2$ composites.

Table 3. Thickness, Solubility, Moisture Content, Water Contact Angle, UTS, and Elongation at Break of SPI-TiO$_2$ Composites[a]

| | | | water droplet contact angle | | | |
samples	thickness (mm)	moisture content (%)	smooth	rough	ultimate tensile strength (MPa)	elongation at break (%)
SPI	0.32 ± 0.001[c]	27.76 ± 1.20[a]	46.71 ± 2.09[b]	80.82 ± 5.45[a]	3.16 ± 0.22[b]	24.25 ± 1.99[e]
0.25%TiO$_2$	0.36 ± 0.002[b,c]	18.95 ± 0.61[c]	59.48 ± 2.44[a]	51.02 ± 0.64[c]	3.47 ± 1.06[a,b]	120.83 ± 2.10[a]
0.5%TiO$_2$	0.38 ± 0.002[a,b,c]	10.10 ± 1.10[d]	38.23 ± 1.06[c]	48.63 ± 3.25[c]	4.58 ± 0.47[a]	95.31 ± 1.50[b]
0.75%TiO$_2$	0.39 ± 0.001[a,b]	17.38 ± 0.22[c]	39.03 ± 4.63[c]	48.85 ± 2.89[c]	3.42 ± 1.25[a,b]	83.53 ± 2.28[c]
1%TiO$_2$	0.42 ± 0.001[a]	22.72 ± 1.12[b]	41.96 ± 0.34[c]	60.01 ± 1.05[b]	2.69 ± 0.12[b]	65.47 ± 3.05[d]

[a]Values are determined as mean ± SD (*n* = 3). Lower case letters (a-e) in the same column indicate significant difference (*p* < 0.05).

320 nm observed in our SPI films was different from the typical SPI emission maximum wavelength of 290 nm. The difference can be attributed to the effects of added glycerol and to the denatured state of SPI. When TiO$_2$ concentration increased from 0.25% to 1%, the fluorescence quenched. Fluorescence quenching in the SPI composite film can be attributed to the formation of a tight tertiary protein structure that can shield the tryptophan residue inside the protein chain.[19] This restricts the free rotation of the internal fluorescence group in the protein, leading to a decrease in fluorescence intensity. This in turn proves that TiO$_2$ addition could alter and strengthen the spatial conformation of the SPI chain, leading to improved functional properties in composite films. A better PL quench is also an indication of better dispersion of the filler in the matrix. Here, the highest quenching was observed in 0.5% TiO$_2$ addition, which shows that TiO$_2$ is uniformly distributed in the SPI matrix at this concentration.

3.5. X-ray Diffraction Analysis. Using the XRD pattern of pure TiO$_2$ (Figure 3C), a rutile characteristic structure was found (2θ = 27°, 36°, 41°, 44°, 54°, 56°, 64°, 70°).[20] The XRD patterns of pure SPI and SPI with lower concentrations of TiO$_2$ (0.25%) show an amorphous nature. When 0.75% TiO$_2$ concentration is present in the film, a clear signal of diffracting peaks appears, indicating the presence of crystalline rutile TiO$_2$ in the SPI crystalline phase. At low TiO$_2$ addition, the coverage of protein on the surface of the TiO$_2$ particles reduced the crystallization characteristics of TiO$_2$, whereas at high TiO$_2$ concentrations, self-assembled large TiO$_2$ cumulations formed could recuperate their crystallization ability.

3.6. FTIR Spectroscopy. The molecular interactions, if any, between the TiO$_2$ and soy protein isolate in the composite films was studied using FTIR spectra. The spectral studies were done also to confirm whether the filler will have any adverse effect on the protein structure or not. In the FTIR spectrum of TiO$_2$ (Figure 4A), a single broad peak below 900 cm^{-1} is attributed to the metal−oxygen (Ti−O) stretching band. The broad peaks at 3188−3428 cm^{-1} and a small peak at 1631 cm^{-1} is attributed to the OH stretching vibrations and bending vibrations of Ti−OH, respectively.[21] All soy protein films exhibited three characteristic amide bands, amide I at 1628
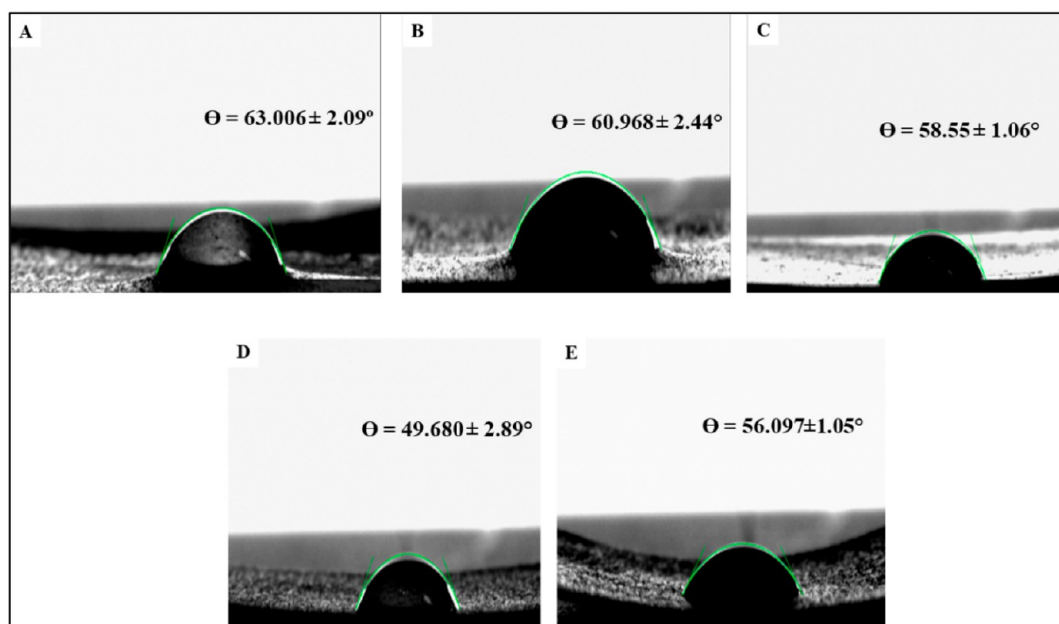
Figure 7. Water contact angle of (A) SPI, (B) 0.25%TiO$_2$, (C) 0.5%TiO$_2$, (D) 0.75% TiO$_2$, and (E) 1%TiO$_2$.
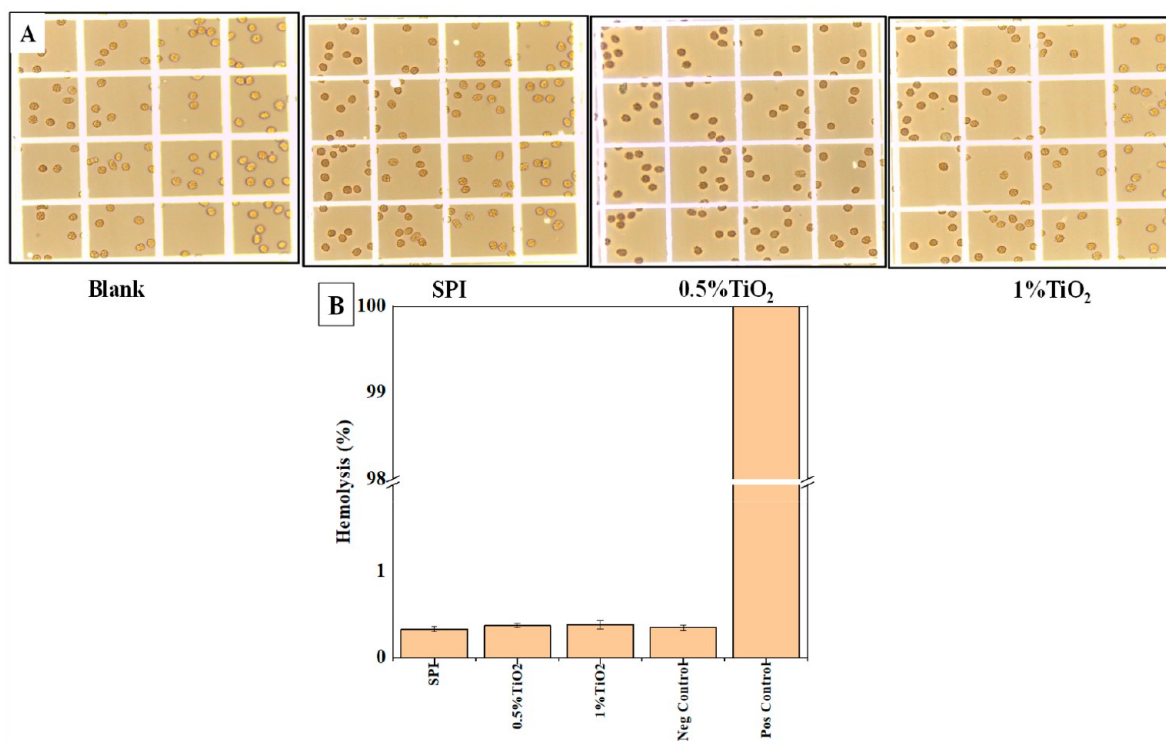

Figure 8. (A) RBC aggregation and (B) percentage of hemolysis in the presence of SPI film scaffolds.

cm^{-1} (C=O stretching), amide II at 1538 cm^{-1} (N–H bending), and amide III at 1136 cm^{-1} (CN stretching), respectively[22−25] (Figure 4B). The addition of the TiO$_2$ into the SPI matrix caused the absorption band of the −OH group to move slightly to a higher wavelength (3264 cm^{-1} to 3271 cm^{-1}). Furthermore, with the addition of 1% TiO$_2$, there occurs a small shift in the absorption intensity of amide I, amide II, and amide III bands, confirming the inclusion of TiO$_2$ in the SPI phase. As reported earlier, the addition of TiO$_2$ normally does not alter the basic protein structure of the SPI matrix. The small variations in the peak height and width

are due to the presence of foreign material in the SPI matrix.[25] Oleyaei et al.[14] have reported that the shift in the absorption peak of C−O bonds to the lower wavelength and the increase in the absorption peak intensity of CH stretching of the methylene group depicts the possibility of electrostatic interactions between the hydroxyl group of starch and TiO$_2$. The slight changes in the spectra obtained can also be attributed to such interactions.

3.7. AFM Analysis. AFM images were used to understand the surface roughness (quantitative) and morphology (qualitative) of composite films. Figure 5 shows the AFM
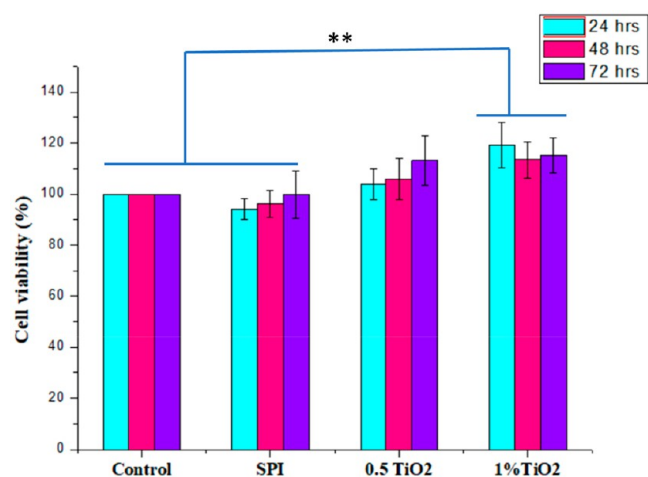
Figure 9. Cell viability of SPI-TiO$_2$ membrane films as determined by MTT assay.

Table 4. Cell Response to SPI Scaffolds after Fourth Week of Subcutaneous Implantation in Rats (Scored by a Blinded Pathologist Using a Four-Point Scoring System (− Absent, + Mild, ++ Moderate, and +++ Severe)

S no.	observations	SPI	0.5% TiO$_2$	1% TiO$_2$
1	angiogenesis	++	+++	++++
2	necrosis	−	−	−
3	lymphocytes	++	+	−
4	pmns	++	−	−
5	giant cells	+	−	−
6	plasma cells	+	−	−
7	overall tissue inflammation response	moderate	low	low

topographic images and a 3D view of the SPI-TiO$_2$ sample surfaces. These images were used to understand the dispersion of TiO$_2$ in the SPI matrix. As expected, differences in surface morphology were observed on the addition of TiO$_2$. The SPI film surface was smooth and uniform. Very distinct surface topology and roughness could be observed from AFM. The variation in height of TiO$_2$ particles dispersed in the SPI matrix can be identified by different color changes in the topography image.

In the AFM image, minimum height (0.37 μm) was observed for the SPI-0.5%TiO$_2$ sample, while pure SPI, SPI-0.25%TiO$_2$, SPI-0.75%TiO$_2$, and SPI-1%TiO$_2$ exhibited height values of 0.46 μm, 0.92 μm, 1.15 μm, and 0.68 μm. The values R_a and R_q represent surface roughness quantitatively. The roughness parameters in the SPI film were 32 and 38 nm. On adding TiO$_2$, the surface roughness decreased up to 0.75% TiO$_2$ addition (27.6 nm (R_a) and 31.8 nm (R_q)) and then increased for 1% TiO$_2$ (52.3 nm (R_a) and 73.8 nm (R_q)). The least surface roughness value was observed for the SPI-0.5% TiO$_2$ sample (21.0 nm (R_a) and 27.4 nm (R_q)). A minimum value of height and surface roughness is an indication of good dispersion of the filler in the matrix. The increase in roughness value with an increase in TiO$_2$ concentration is due to agglomeration of TiO$_2$ in the SPI matrix.

3.8. IGC Analysis. *3.8.1. Surface Energy.* The dispersive surface energy, adsorption potential maxima (A_{max}), and K_a/K_b values of the SPI-TiO$_2$ samples are shown in Table 2. The Υ_S^d values of the composite samples were not statistically different

from the control and ranged from 38.43 to 35.30 mJ/m^2. For the soy samples, upon using TiO$_2$, it made the resulting composites more energetic (increased total surface energy up to 17%), resulting from the increase of the specific surface energy. The increment of the surface energy with the addition of TiO$_2$ could result from changes in the fiber conformation during the manufacturing process, which led to higher interaction with polar probes. Even though similar Υ_S^d values ($p < 0.05$) were obtained between samples, the number and/or energy of the active sites could have changed. Thus, the heterogeneity profile was evaluated with the aim of accessing the active sites found at the surface (Figure 6A). Regarding the heterogeneity profile, some changes can be observed. At lower TiO$_2$ amounts (0.25% and 0.50%), the plot depicts a similar number (y axis) and energy (x axis) of the active sites. In the case of the samples with higher TiO$_2$ amounts, a significant decrease in the energy of the active sites is observed (A_{max} values decrease by 20%), which agrees with the decrease of the Υ_S^d value.

Even though similar Υ_S^d values were obtained between samples, the number and/or energy of the active sites could have changed. Thus, the heterogeneity profile was evaluated with the aim of accessing the active sites found at the surface. At lower TiO$_2$ amounts (0.25% and 0.50%), the plot depicts a similar number (y axis) and energy (x axis) of the active sites. In the case of the samples with higher TiO$_2$ amounts, a significant decrease in the energy of the active sites is observed (A_{max} values decrease up to 20%), which agrees with the decrease in the Υ_S^d value.

3.8.2. Polar Interactions. As seen through the analysis of the surface energy in the SPI samples, with the addition of TiO$_2$, the surface energy increased due to the increased polar interactions. This way, the Gibbs free energy of adsorption of different polar probes for the SPI-TiO$_2$ was assessed, which can be found in Figure 6B. With the incorporation of TiO$_2$, an increased interaction with the basic probes (ethyl acetate and THF) is observed, which translates into an increased acidic surface nature (higher K_a/K_b). Moreover, the interactions with dichloromethane (an acid probe) decreased, which further verifies the decrease of the surface basicity. It is most likely that variations in the polymeric chain orientation happened during the production of the membranes, which caused changes in the interactions with the polar probe molecules and, consequently, changes in the acid−base character. Due to the low amounts of TiO$_2$ used in the experiment, it is expected that it should not impact significantly the interactions with the probes under study.

3.8.3. Diffusion. The samples were subjected to diffusion analysis, using *n*-octane as the probe, and the parameter (D_p) can be found in Table 2. With the introduction of TiO$_2$, in SPI samples, the D_p is substantially increased. This indicates that the probe could cross much faster through the samples, indicating that a higher porosity was obtained in the presence of TiO$_2$ during the manufacture of the membranes. Increased surface porosity and diffusion values indicate the potential applicability of the film samples as a wound dressing material since it will permit the passage of oxygen to the wounded area, thus helping in maintaining optimum oxygen concentration to promote healing.

3.9. Film Thickness. The thickness of the final film is an important parameter which affects the migration rate of the liquid film-forming dispersion and hence is crucial for the mechanical and barrier properties of the films. Normally, film
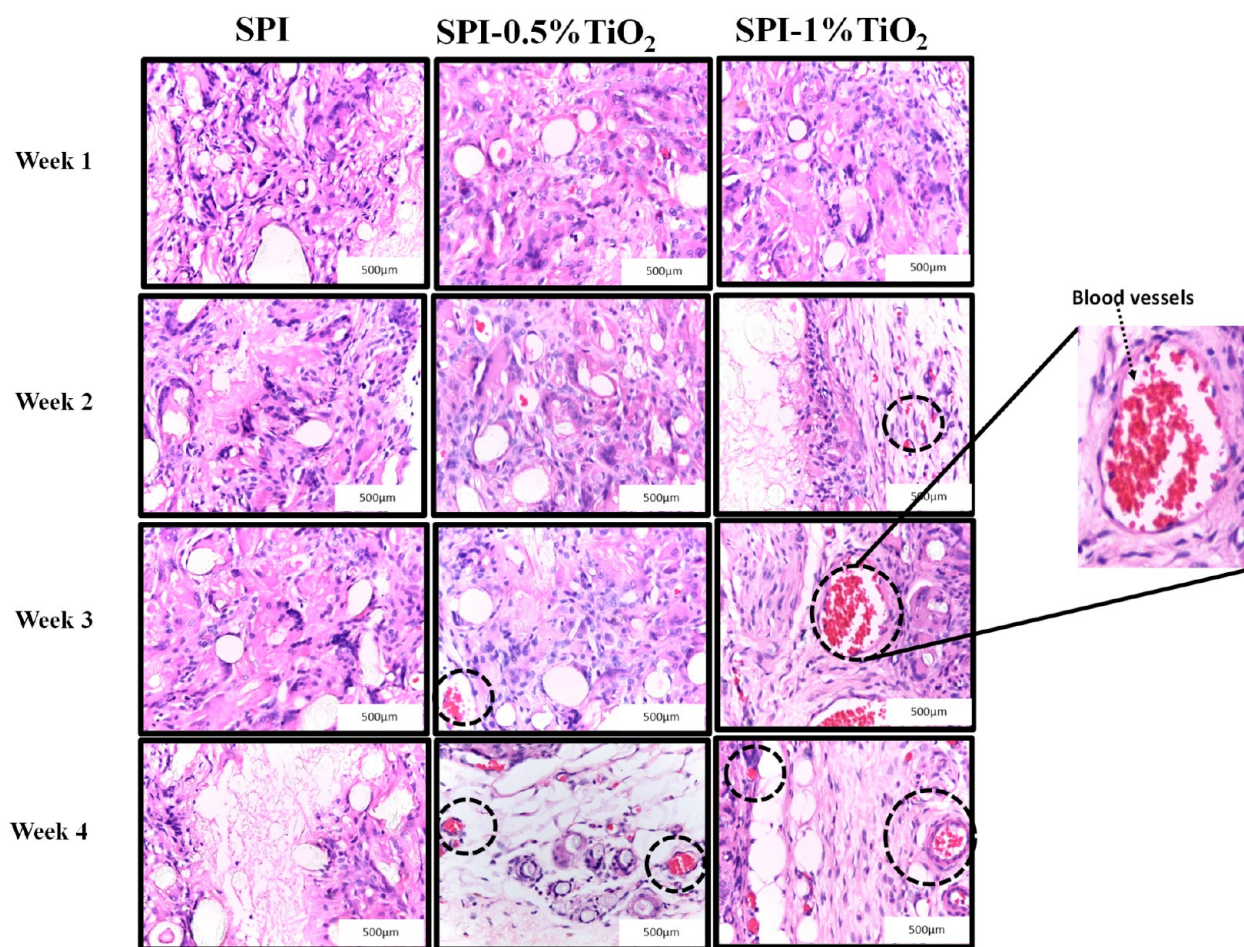
Figure 10. Histology analysis of SPI membranes after in vivo implantation for showing the formation of blood vessels through implanted films (the circles represent the blood cells grown on the scaffold that represents angiogenesis).

thickness depends on the nature of film components, composition of the film-forming solution, preparation methods, drying conditions, etc. The thickness values of the SPI-TiO$_2$ composite are shown in Table 3. Film thickness was found to be in the range 0.032−0.04 mm. This indicated that the thickness values of SPI-TiO$_2$ composite films increased with an increase in the TiO$_2$ content. The results suggested that the alignment of SPI peptide chains in the film matrix was formed with a lower degree of compactness, when the increased content of TiO$_2$ was incorporated. The dispersed TiO$_2$ microparticles might have inserted themselves between SPI molecules of the film matrix, thereby hindering the interaction within the peptide chains.[22]

3.10. Mechanical Properties. The stress−strain curves of SPI and SPI-TiO$_2$ films are shown in Figure 6C. A simultaneous enhancement in the tensile strength and elongation at break values was obtained with the addition of TiO$_2$ to the SPI matrix. As shown in the figure, the mechanical properties of the SPI films increased with the addition of TiO$_2$ up to 0.5% and then decreased. The film's tensile strength is shown in Table 3. The tensile strength of the control SPI film was amplified and reached a maximum of 4.58 MPa with the TiO$_2$ concentration increased from 0 to 0.5% ($p < 0.05$). This shows that the addition of TiO$_2$ particles into the matrix solution resulted in strong interfacial interaction within the matrix network via the formation of covalent and hydrogen bonds. On further addition of TiO$_2$ from 0.75% to 1%, there

was a significant decrease in the tensile strength, which may be due to the accumulation of TiO$_2$ particles in the matrix. This clearly shows that the uniform distribution of the microfiller in the matrix results in a specific and effective transfer of stress from the matrix to the filler, resulting in the increased strength of the film. The elongation at the break value was significantly ($p < 0.05$) increased with the addition of TiO$_2$. In fact, the addition of 0.25% TiO$_2$ was found to enhance the elongation at the break value by 120.83%. Balasubramanian et al.[26] have also reported that the addition of TiO$_2$ increased the elongation at the break value of biopolymeric films.

3.11. Thermogravimetric Analysis. The thermal stability of the prepared SPI-TiO$_2$ composite films was analyzed by thermogravimetry. The thermogram (Figure 6D) revealed that all of the films exhibited similar degradation trends. A three-step degradation pattern was observed for all of the films. The first stage (70−100 °C) can be assigned to the loss of H$_2$O. The second stage between 100 and 250 °C is assigned to the loss of the plasticizer. The third stage occurs between 250 and 400 °C and is assigned to the breakdown of the protein backbone and other fillers. The total weight loss of SPI was 90.15%. The addition of TiO$_2$ was found to increase the thermal stability of SPI film. The temperature at which 50% weight loss in the SPI-1%TiO$_2$ composite film occurred was 322.66 °C, while for the control SPI film it was 309.16 °C. The decreased weight loss at lower temperatures on adding TiO$_2$ can be attributed to the high thermal stability of TiO$_2$ particles.

Oleyaei et al.[14] have also reported an increase in the thermal stability of chitosan film on adding TiO_2 particles. The residual masses of SPI, SPI-0.25%, SPI-0.5%, SPI-0.75%, and SPI-1% TiO_2 films were 15.21%, 17.23%, 18.89%, 19.15%, and 19.17%, respectively. This shows that the addition of TiO_2 can protect the film from losing weight by hindering the diffusion of volatile products of SPI, thus maintaining the integrity of films at high temperatures.

3.12. Moisture Content. Water sensitivity is one of the major problems of SPI-based films, which has limited their application. The pure SPI film had the highest moisture content. The moisture content of SPI/TiO_2 films was found to decrease with the increased addition of TiO_2 with 0.5%TiO_2 addition giving a 64% reduction (Table 3). This result was ascribed to TiO_2 getting trapped inside the SPI matrix, restricting the entry of water molecules, which resulted in decreased moisture content. In addition, the addition of micro-TiO_2 into the SPI matrix could cause strong hydrogen bonds to form between the two main components, which could prevent water diffusing through the films, thus reducing moisture content values. However, when more than 0.5 wt % of TiO_2 was included, it aggregated to result in decreased effective filler dispersion in the polymer matrix and facilitated moisture permeation.

3.13. Wettability Properties. The water contact angle is a physical quantity which determines the surface wettability or hydrophilicity of the film. The surface wettability or hydrophilicity is an important parameter to be considered when selecting materials for skin scaffolds. It has a direct connection with cell proliferation and attachment. A low contact angle value indicates good surface wettability and hence hydrophilic character. The water contact angle of SPI and SPI-TiO_2 composite films is shown in Figure 7. SPI itself is hydrophilic since it has a contact angle of 63.76°, which is below the standard value of 90° expected for a hydrophobic material. The contact angle values that are suitable for such applications are normally between 30 and 70°. The addition of TiO_2 to the SPI matrix was found to decrease the surface contact angle or increase the surface wettability. The contact angle values decreased on adding TiO_2 up to 0.75% (43.94°). On adding 1% TiO_2, the water contact angle slightly increased to 50.985°. A similar trend in contact angle values was observed by Oleyaei et al.,[14] when TiO_2 was incorporated in starch film. This result is in agreement with the high surface energy results obtained from IGC measurements, as it has been reported by Chamas et al.,[27] that high surface energy will generally cause good wetting and a low contact angle. The slight increase in the contact angle value of the SPI-1%TiO_2 sample is also in agreement with the increase in surface roughness values obtained from AFM and SEM. It has been reported by Quetzeri-Santiago et al.[28] that an increase in the surface roughness results in an increase of the maximum dynamic contact angle θ_{max}. These hydrophilic films can be used as a wound dressing agent since they help in maintaining a moist wound environment, which is essential for rapid healing of the wound.

3.14. Blood Compatibility. Tissue engineering scaffolds are directly implanted in the body, and they have direct contact with the blood. Hence, such material should not have any adverse effect on the functioning of RBCs upon contact. The results obtained show no visible RBC aggregation (Figure 8A) after incubating the film extract with RBCs. With the SPI and SPI-TiO_2 films, there was no chance of aggregation of the blood cells. Also, no change in the size and shape of the blood

cells indicates that the scaffold materials are not imparting any harm to the cells. Hemolysis studies are also important in assessing the compatibility of the material with blood. The hemolysis assay (Figure 8B) performed on all film extracts revealed a minimum hemolytic potential within an acceptable limit of 1%. There was no statistical difference between the negative control and the film extracts, while a huge difference was observed between the studied samples and the positive control.

3.15. Biocompatibility of SPI Composite Films. Cell viability studies were performed to test the biocompatibility of SPI-TiO_2 composite film membranes. Results of an MTT cell proliferation assay on SPI, SPI-0.5%TiO_2, and SPI-1%TiO_2 films after 24, 48, and 72 h of cell culture are shown in Figure 9. Mouse fibroblast cells (L929 cells) seeded on all SPI films and SPI-TiO_2 films showed more than 96% cell viability over the whole cell culture periods of 24, 48, and 72 h. Even the control SPI membranes showed 98% cell viability. All of the materials showed a cell viability of more than 90%, which is fairly acceptable per the available literature. Very interestingly, L929 cells seeded on SPI-1%TiO_2 membranes showed 118% cell viability ($p < 0.05$). The cell viabilities of all three SPI films, control SPI, SPI-0.5%TiO_2, and SPI-1%TiO_2 membranes were significantly higher than the untreated control.

When considering the results after 24 h as the control and on comparing the cell proliferation, it is clear that the cells treated with SPI-0.5%TiO_2 show enhanced viability while the cells treated with SPI-1%TiO_2 showed a slight decrease, but within the acceptable limit. According to the findings, the incorporation of TiO_2 in the SPI allows the cell growth. The SPI film surface is also suitable for the growth of the live cells. The small decrease in the viability rate after 72 h for the TiO_2 (1%) films can be attributed to the roughness in the surface of the film as evident from the SEM images. The particle per unit space is more in the SPI-TiO_2 (1%) composites, hence it slightly decreases the space for proper growth. However, the distribution of the microfiller is not so uniform that still there is enough space for the cells for healthy living and proliferation.[29,30] The results show that the viability of the cells for all membranes prepared in this experiment was excellent on the whole, showing no cytotoxicity.

3.16. Histopathological Analysis after Subcutaneous Implantation in Adult Male Sprague−Dawley Rats. Usually, when a foreign body is implanted in vivo, it can result in an inflammatory response. A mild pro-inflammatory response facilitates tissue regeneration, while an unnecessary provocative response leads to organ impairment or abnormalities. Hence, it is important to study the in vivo performance of the material after implanting in animal bodies.[31] Preclinical behavior of the prepared film membranes was studied using the subcutaneous implantation model. SPI and SPI-TiO_2 film membranes were subcutaneously implanted into male Sprague−Dawley rats for 4 weeks, and the inflammatory response, cell proliferation, and angiogenesis on the scaffolds at the end of the first, second, third, and fourth weeks of implantation were monitored (Table 4). The rats remained perfectly fine throughout the experiment without any mortality or abnormal behavior, suggesting the absence of toxicity on account of scaffold implantation. No sign of necrosis was observed in the neat SPI or SPI-TiO_2 scaffold groups throughout the study period. The healing of a scar or wound progresses through four stages in which there are platelets, neutrophils, fibroblasts, and epithelium. The fibroblast and

angiogenesis represent the proliferation stage and are considered an indication of healing.[32] Superior angiogenic responses compared to the bare SPI samples were observed in SPI-0.5%TiO$_2$ and SPI-1%TiO$_2$. There was a significant difference in histological scores among the SPI membrane (blank) and SPI-TiO$_2$ membranes in terms of angiogenesis, lymphocytes, polymorphonuclear leukocytes (PMNs), giant cells, plasma cells, and overall tissue inflammation response at different time points.

Interestingly, just after 1 week of implantation, angiogenesis was observed on the SPI-TiO$_2$ membrane scaffolds (Figure 10). Only very few lymphocytes and giant cells were seen. PMNs were rare. Earlier studies[33] have proved that ultra-sonication on TiO$_2$ particles promoted neovascularization in rat models, which is attributed to the generation of reactive oxygen species (ROS) by TiO$_2$ in biological systems. The metal oxide fillers have been proven to be effective in inducing cell proliferation and angiogenesis, and the mechanism has been explained by Augustine et al.[34,35] Reduction of inflammatory cells and induction of angiogenesis response in the SPI scaffold with TiO$_2$ at the fourth week give evidence to the biocompatibility of the membrane.

■ CONCLUSION

The foremost intentions of this work were to investigate (1) the effect of the sonication on the dispersion property of TiO$_2$ and (2) the effect of addition of the sonicated TiO$_2$ on the physiochemical properties of SPI films. It was found that sonication could enhance the dispersion of TiO$_2$ in the matrix, and by adjusting the concentration of TiO$_2$ microparticles, the properties of the TiO$_2$/SPI composite film could be tailored. The SPI-TiO$_2$ films possessed a decreased transmittance in the UVA and visible regions and fluorescence quenching, which promoted its photocatalytic antibacterial effects. The mechanical strength and thermal stability of SPI films were enhanced in the presence of TiO$_2$. The surface roughness, wettability, surface energy, and diffusion coefficient were significantly enhanced with the addition of TiO$_2$. Biocompatibility studies showed 118% L929 cell growth on SPI-1%TiO$_2$ scaffold. An in vivo implantation study demonstrated that TiO$_2$ containing SPI membranes can enhance angiogenesis in the implantation site. Overall, the study indicated that SPI membrane scaffolds containing TiO$_2$ can be used as a base material for the development of biodegradable scaffolds for wound healing applications. However, further investigations on teratogenicity, genotoxicity, and carcinogenicity need to be done to rule out any long-term adverse effects of the developed membrane scaffolds.

■ ASSOCIATED CONTENT

ⓢ Supporting Information

The Supporting Information is available free of charge at https://pubs.acs.org/doi/10.1021/acsbiomaterials.2c00548.

    Water uptake studies (PDF)

■ AUTHOR INFORMATION

Corresponding Author

    Laly A. Pothen − *Department of Chemistry, CMS College, M G University, Kottayam 686001 Kerala, India;* Phone: 9497785727; Email: lapothen@gmail.com

Authors

    Rekha Rose Koshy − *Postgraduate and Research Department of Chemistry, Bishop Moore College, University of Kerala, Mavelikara 690101 Kerala, India; Department of Chemistry, CMS College, M G University, Kottayam 686001 Kerala, India*

    Siji K. Mary − *Postgraduate and Research Department of Chemistry, Bishop Moore College, University of Kerala, Mavelikara 690101 Kerala, India; Department of Chemistry, CMS College, M G University, Kottayam 686001 Kerala, India*

    Arunima Reghunadhan − *Department of Chemistry, TKM College of Engineering, Kollam 691005 Kerala, India;* ⓞ orcid.org/0000-0003-3658-3589

    Yogesh Bharat Dalvi − *Pushpagiri Research Centre, Pushpagiri Institute of Medical Sciences, Tiruvalla, Kerala 689101, India*

    Lekshmi Kailas − *School of Physics and Astronomy, University of Leeds, LS2 9JT London, United Kingdom*

    Nereida Cordeiro − *Faculty of Science and Engineering, University of Madeira, 9000-390 Funchal, Portugal*

    Sabu Thomas − *School of Energy Materials, Mahatma Gandhi University, Kottayam, Kerala 686560, India*

Complete contact information is available at:
https://pubs.acs.org/10.1021/acsbiomaterials.2c00548

Notes

The authors declare no competing financial interest.

■ REFERENCES

(1) Tarrahi, R.; Khataee, A.; Karimi, A.; Yoon, Y. The Latest Achievements in Plant Cellulose-Based Biomaterials for Tissue Engineering Focusing on Skin Repair. *Chemosphere* **2022**, *288*, 132529.

(2) Yang, Q.; Peng, J.; Xiao, H.; Xu, X.; Qian, Z. Polysaccharide Hydrogels: Functionalization, Construction and Served as Scaffold for Tissue Engineering. *Carbohydr. Polym.* **2022**, *278*, 118952.

(3) Negrescu, A.; Mitran, V.; Draghicescu, W.; Popescu, S.; Pirvu, C.; Ionascu, I.; Soare, T.; Uzun, S.; Croitoru, S. M.; Cimpean, A. TiO$_2$ Nanotubes Functionalized with Icariin for an Attenuated In Vitro Immune Response and Improved In Vivo Osseointegration. *J. Funct. Biomater.* **2022**, *13*, 43.

(4) Xie, J.; Hung, Y. C. UV-A Activated TiO2 Embedded Biodegradable Polymer Film for Antimicrobial Food Packaging Application. *Lwt* **2018**, *96*, 307−314.

(5) Bui, V. K. H.; Tran, V. V.; Moon, J.-Y.; Park, D.; Lee, Y.-C. Titanium Dioxide Microscale and Macroscale Structures: A Mini-Review. *Nanomaterials* **2020**, *10* (6), 1190.

(6) Zhao, Y.; Wang, Z.; Zhang, Q.; Chen, F.; Yue, Z.; Zhang, T.; Deng, H.; Huselstein, C.; Anderson, D. P.; Chang, P. R.; Li, Y.; Chen, Y. Accelerated Skin Wound Healing by Soy Protein Isolate−Modified Hydroxypropyl Chitosan Composite Films. *Int. J. Biol. Macromol.* **2018**, *118*, 1293−1302.

(7) Ma, M.; He, W.; Liu, X.; Zheng, Y.; Peng, J.; Xie, Y.; Meng, H.; Wang, Y. Soybean Protein Isolate/Chitosan Composite Microcarriers for Expansion and Osteogenic Differentiation of Stem Cells. *Compos. Part B Eng.* **2022**, *230*, 109533.

(8) Suarato, G.; Bertorelli, R.; Athanassiou, A. Borrowing from Nature: Biopolymers and Biocomposites as Smart Wound Care Materials. *Front. Bioeng. Biotechnol* **2018**, *6*, 137.

(9) Mei, S.; Yang, L.; Pan, Y.; Wang, D.; Wang, X.; Tang, T.; Wei, J. Influences of Tantalum Pentoxide and Surface Coarsening on Surface Roughness, Hydrophilicity, Surface Energy, Protein Adsorption and Cell Responses to PEEK Based Biocomposite. *Colloids Surfaces B Biointerfaces* **2019**, *174*, 207−215.

(10) Maleki, A.; He, J.; Bochani, S.; Nosrati, V.; Shahbazi, M.-A.; Guo, B. Multifunctional Photoactive Hydrogels for Wound Healing Acceleration. *ACS Nano* 2021, 15 (12), 18895−18930.

(11) Alonso, E.; Faria, M.; Ferreira, A.; Cordeiro, N. Influence of the Matrix and Polymerization Methods on the Synthesis of BC/PANi Nanocomposites: An IGC Study. *Cellulose* 2018, 25 (4), 2343−2354.

(12) Nair, S. B.; Jyothi, A. N.; Sajeev, M. S.; Misra, R. Rheological, Mechanical and Moisture Sorption Characteristics of Cassava Starch-Konjac Glucomannan Blend Films. *Starch/Stärke* 2011, 63, 728−739.

(13) Augustine, R.; Dalvi, Y. B.; Dan, P.; George, N.; Helle, D.; Varghese, R.; Thomas, S.; Menu, P.; Sandhyarani, N. Nanoceria Can Act as the Cues for Angiogenesis in Tissue-Engineering Scaffolds: Toward Next-Generation in Situ Tissue Engineering. *ACS Biomater. Sci. Eng.* 2018, 4 (12), 4338−4353.

(14) Oleyaei, S. A.; Zahedi, Y.; Ghanbarzadeh, B.; Moayedi, A. A. Modification of Physicochemical and Thermal Properties of Starch Films by Incorporation of TiO2 Nanoparticles. *Int. J. Biol. Macromol.* 2016, 89, 256−264.

(15) Gu, W.; Liu, X.; Li, F.; Shi, S. Q.; Xia, C.; Zhou, W.; Zhang, D.; Gong, S.; Li, J. Tough, Strong, and Biodegradable Composite Film with Excellent UV Barrier Performance Comprising Soy Protein Isolate, Hyperbranched Polyester, and Cardanol Derivative. *Green Chem.* 2019, 21 (13), 3651−3665.

(16) Han, Y.; Yu, M.; Wang, L. Preparation and Characterization of Antioxidant Soy Protein Isolate Films Incorporating Licorice Residue Extract. *Food Hydrocoll* 2018, 75, 13−21.

(17) Goudarzi, V.; Shahabi-Ghahfarrokhi, I.; Babaei-Ghazvini, A. Preparation of Ecofriendly UV-Protective Food Packaging Material by Starch/TiO2 Bio-Nanocomposite: Characterization. *Int. J. Biol. Macromol.* 2017, 95, 306−313.

(18) Li, Y.; Jiang, Y.; Liu, F.; Ren, F.; Zhao, G.; Leng, X. Fabrication and Characterization of TiO2/Whey Protein Isolate Nanocomposite Film. *Food Hydrocoll* 2011, 25 (5), 1098−1104.

(19) Xiao, Y.; Liu, Y.; Kang, S.; Xu, H. Insight into the Formation Mechanism of Soy Protein Isolate Films Improved by Cellulose Nanocrystals. *Food Chem.* 2021, 359, 129971.

(20) Ahmadi, R.; Tanomand, A.; Kazeminava, F.; Kamounah, F. S.; Ayaseh, A.; Ganbarov, K.; Yousefi, M.; Katourani, A.; Yousefi, B.; Samadi Kafil, H. Fabrication and Characterization of a Titanium Dioxide (TiO2) Nanoparticles Reinforced Bio-Nanocomposite Containing Miswak (Salvadora Persica L.) Extract − The Antimicrobial, Thermo-Physical and Barrier Properties. *Int. J. Nanomedicine* 2019, 14, 3439−3454.

(21) Razali, M. H.; Ismail, N. A.; Mat Amin, K. A.Titanium Dioxide Nanotubes Incorporated Gellan Gum Bio-Nanocomposite Film for Wound Healing: Effect of TiO2 Nanotubes Concentration*Int. J. Biol. Macromol..* 2020. 1531117.

(22) Ahmad, M.; Nirmal, N. P.; Danish, M.; Chuprom, J.; Jafarzedeh, S. Characterisation of Composite Films Fabricated from Collagen/Chitosan and Collagen/Soy Protein Isolate for Food Packaging Applications. *R. Soc. Chem.* 2016, 6 (85), 82191−82204.

(23) Dash, S.; Swain, S. K. Effect of Nanoboron Nitride on the Physical and Chemical Properties of Soy Protein. *Composites Science and Technology* 2013, 84, 39−43.

(24) Wang, X.; Chi, Y. Microwave-Assisted Phosphorylation of Soybean Protein Isolates and Their Physicochemical Properties. *Czech J. Food Sci.* 2012, 30 (2), 99−107.

(25) Wang, S.-Y.; Zhu, B.-B.; Li, D.-Z.; Fu, X.-Z.; Shi, L. Preparation and Characterization of TIO2/SPI Composite Film. *Mater. Lett.* 2012, 83, 42−45.

(26) Balasubramanian, R.; Kim, S. S.; Lee, J.; Lee, J. Effect of TiO 2 on Highly Elastic, Stretchable UV Protective Nanocomposite Films Formed by Using a Combination of k-Carrageenan, Xanthan Gum and Gellan Gum. *Int. J. Biol. Macromol.* 2019, 123, 1020−1027.

(27) Chamas, A.; Moon, H.; Zheng, J.; Qiu, Y.; Tabassum, T.; Jang, J. H.; Abu-Omar, M.; Scott, S. L.; Suh, S. Degradation Rates of Plastics in the Environment. *ACS Sustain. Chem. Eng.* 2020, 8 (9), 3494−3511.

(28) Quetzeri-Santiago, M. A.; Castrejón-Pita, A. A.; Castrejón-Pita, J. R. The Effect of Surface Roughness on the Contact Line and Splashing Dynamics of Impacting Droplets. *Sci. Rep* 2019, 9 (1), 1−10.

(29) Pattanashetti, N. A.; Hiremath, C.; Naik, S. R.; Heggannavar, G. B.; Kariduraganavar, M. Y. Development of Nanofibrous Scaffolds by Varying the TiO2 Content in Crosslinked PVA for Bone Tissue Engineering. *New J. Chem.* 2020, 44 (5), 2111−2121.

(30) Jayakumar, R.; Ramachandran, R.; Divyarani, V. V.; Chennazhi, K. P.; Tamura, H.; Nair, S. V. Fabrication of Chitin-Chitosan/Nano TiO2-Composite Scaffolds for Tissue Engineering Applications. *Int. J. Biol. Macromol.* 2011, 48 (2), 336−344.

(31) Ninan, N.; Joseph, B.; Visalakshan, R. M.; Bright, R.; Denoual, C.; Zilm, P.; Dalvi, Y. B.; Priya, P. V.; Mathew, A.; Grohens, Y.; Kalarikkal, N.; Vasilev, K.; Thomas, S. Plasma Assisted Design of Biocompatible 3D Printed PCL/Silver Nanoparticle Scaffolds: In Vitro and in Vivo Analyses. *Mater. Adv.* 2021, 2 (20), 6620−6630.

(32) Yu, R.; Zhang, H.; Guo, B.*Conductive Biomaterials as Bioactive Wound Dressing for Wound Healing and Skin Tissue Engineering*; Springer: Singapore, 2022; Vol. 14. DOI: 10.1007/s40820-021-00751-y.

(33) Augustine, R.; Hasan, A.; Patan, N. K.; Augustine, A.; Dalvi, Y. B.; Varghese, R.; Unni, R. N.; Kalarikkal, N.; Al Moustafa, A. E.; Thomas, S. Titanium Nanorods Loaded PCL Meshes with Enhanced Blood Vessel Formation and Cell Migration for Wound Dressing Applications. *Macromol. Biosci.* 2019, 19 (7), e1900058.

(34) Augustine, R.; Mathew, A. P.; Sosnik, A. Metal Oxide Nanoparticles as Versatile Therapeutic Agents Modulating Cell Signaling Pathways: Linking Nanotechnology with Molecular Medicine. *Appl. Mater. Today* 2017, 7, 91−103.

(35) Augustine, R.; Dominic, E. A.; Reju, I.; Kaimal, B.; Kalarikkal, N.; Thomas, S. Investigation of Angiogenesis and Its Mechanism Using Zinc Oxide Nanoparticle-Loaded Electrospun Tissue Engineering Scaffolds. *RSC Adv.* 2014, 4 (93), 51528−51536.

🔲 Recommended by ACS